Reduction of O2 to H2O2 using Small Polycyclic Molecules

Journal:	*Catalysis Science & Technology*
Manuscript ID	CY-ART-02-2021-000244.R1
Article Type:	Paper
Date Submitted by the Author:	10-Jun-2021
Complete List of Authors:	Lopez, Kristal; California State University Fullerton Department of Chemistry and Biochemistry, Chemistry and Biochemistry Groves, Michael; California State University Fullerton Department of Chemistry and Biochemistry, Chemistry and Biochemistry

Journal Name

A Computational Study on the Reduction of O_2 to H_2O_2 using Small Polycyclic Aromatic Molecules[†]

Kristal Lopez,[a] and Michael N Groves[*a]

Hydrogen peroxide is an environmentally friendly oxidizing agent that is important in several industries. It is currently produced industrially via the anthrahydroquinone (AHQ) process where O_2 reacts with a functionalised version of anthrahydroquinone to produce H_2O_2 and anthraquinone. In the previously published DFT pathway for this process the transition of the OOH· radical across the partially dehydrogenated AHQ catalyst was not explored. In this paper, we will use DFT to explore this step and show that there is a deep potential energy minimum that inhibits the OOH· from being fully reduced. We then examine other similar sized polycyclic molecules with two OH-groups on the same side that could serve as alternative catalysts without this issue. In this analysis, we identify phenanthraquinone as a possible alternative and present the pathway for this candidate to produce H_2O_2 as well as its regeneration with H_2.

1 Introduction

Hydrogen peroxide (H_2O_2) is used in many industries including as a bleaching agent for paper production[1–5] and water treatment[6–8]. Worldwide production exceeds 5.5 million metric tons in 2015 and it continues to climb[3]. It is also used in several other applications including the synthesis of organic chemicals such as Propylene Oxide through the hydrogen peroxide propylene oxide (HPPO) process where hydrogen peroxide is used as the oxidant[9,10]. HPPO is the integration of two processes: first the anthraquinone (AQ) process synthesizes hydrogen peroxide and is then integrated with the propene epoxidation process catalyzed by titanium silicalite[11]. Hydrogen peroxide can also serve as an alternative energy carrier in fuel cell applications. Fuel cells traditionally use oxygen as the oxidant, but in a recent investigation H_2O_2 was used not only as an alternative oxidant but as a reductant making the cell structure simpler[12]. Theoretically, it would provide a higher power output compared to fuel-cells where oxygen is the oxidant.

There are multiple ways under study to synthesize H_2O_2. The $2e^-$ electrochemical processes has recently been gaining in popularity. The focus has been on a water electrolyzer configuration instead of a hydrogen-based fuel cell type system due to the high cost and storage of H_2 gas[13]. In this system, metallic[14–17] and non-metallic[18–22] electrode materials have been studied. A second method to synthesize H_2O_2 is direct synthesis from H_2/O_2 mixtures in a high-pressure gas like CO_2 or N_2. In these cases,

a Pd-based catalyst is used and the high-pressure gas is meant to limit the fire hazard given the explosive nature of H_2/O_2 mixtures as well as the inclusion of methanol as a solvent[13]. Supercritical CO_2 has also been explored as a solvent to replace methanol, however, the reaction temperature plays a significant role. In a study by Landon *et al.* they observed that the critical temperature of CO_2 was high enough to promote a high decomposition rate of H_2O_2. They found that temperatures around 274 K with Pd-Au catalysts and methanol as the solvent results in high yields of H_2O_2[23]. A third method to synthesize hydrogen peroxide is via the gas-phase reaction of a H_2/O_2 non-equilibrium plasma[24,25]. This method has the benefit of not needing any catalysts or added chemicals, however, it does not draw much attention over safety concerns. A double dielectric barrier discharge reactor can safely work with 30 mol% O_2 content[26] which is much higher than the typical 6% explosion limit[27]. A fourth method involves the UV illumination of an aqueous suspension of TiO_2 particles. The efficiency of this photochemical process can be significantly improved with the addition of Cu^{2+}[28]. However, the most common way to synthesize H_2O_2 is via the AQ process[29], which is illustrated in Figure 1. In industry, the majority of H_2O_2 is produced using the AQ process. It consists of two processes: the hydrogenation process and the autoxidation process[29]. H_2O_2 is synthesized in the autoxidation step and the catalyst is regenerated with H_2 on a Pd catalyst to form anthrahydroquinone (AHQ). This process is energy intensive and damages the environment so until a scalable alternative exists it is important to examine and improve the current process to minimize these effects.

In this project, the focus is on the autoxidation step in the AQ process. In the autoxidation step, the triplet O_2 and AHQ produce singlet H_2O_2 and AQ under ambient conditions. In a pre-

a California State University, Fullerton, Fullerton, CA, 92831, USA. Fax: +1(657)278-5316; Tel: +1(657)278-7018; E-mail: mgroves@fullerton.edu
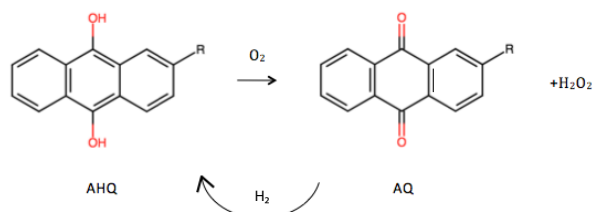
Fig. 1 The overall anthraquinone process. The second half of the reaction is known as the autoxidation step.

vious study, density functional theory was used to examine the the autoxidation step of the AQ process[2]. In this work a crucial step is missing where the hydroperoxyl (OOH·) radical transitions across the partially dehydrogenated AHQ molecule to perform the second hydrogen abstraction. Given that the overall AQ process is still being determined[30,31], the goal of this investigation is to calculate the transition of the OOH· across the AHQ molecule in an effort to examine one of many possibilities so that an accurate representation of this process can be determined. It was found that this transition has a deep potential well in the singlet state that probably acts as the rate-determining step as the OOH· transitions across the AHQ molecule. Alternative catalysts will be explored with both OH-groups on the same side of the molecule, which eliminates the need for the intermediate to move across the catalyst. Phenanthraquinone has been identified as an alternative catalyst, and the barriers of the autoxidation and hydrogenation steps will be presented and compared to those from AHQ to reduce O_2 to H_2O_2.

2 Methods

All calculations are performed using the Python-based density functional theory (DFT) software GPAW[32,33] supported by the Atomic Simulation Environment (ASE)[34]. The generalized gradient approximation (GGA) using the Perdew, Burke, and Ernzerhof (PBE)[35] exchange-correlation functional was used. Dispersion interactions were taken into account using the Tkatchenko-Scheffler method[36]. All reported results use a Monkhorst-Pack $\vec{k}$-point mesh of $2 \times 2 \times 1$ in a $12.78\text{Å} \times 14.757\text{Å} \times 20.45\text{Å}$ cell, and a grid spacing below 0.1775 based on a convergence test presented in Table S1. Molecular geometries are relaxed to a maximum force less than 0.02 eV/Å. In this project, the O_2 system has a triplet spin, and the H_2O_2 has a singlet spin; therefore, reaction pathways with both spins are calculated. This accomplished by performing spin polarized calculations where the magnetic moment is fixed to 2.0 for triplet state calculations, and 0.0 for the singlet state calculations.

Reaction barriers are calculated between intermediates to find the transition states. The nudged elastic band (NEB) method is used to find minimum energy paths (MEP)[37]. The automated nudged elastic band (AutoNEB) algorithm is an add-on to the basic NEB method that effectively locates transition states because it focuses resources to better characterize less resolved regions along the MEP[38]. The AutoNEB runs with the same basic NEB algorithm, where it will initialize a pathway with a user designated number of images, however, it then iteratively adds and relaxes more images until a predetermined total number of images is achieved. This converges a rough pathway and once the region around the saddle point is resolved, a climbing image is used to converge the transition state[38].

3 Results and discussion

The calculated reaction pathway for reducing O_2 to H_2O_2 is shown in Figure 2. All reported energies for Figure 2 use the separated O_2/AHQ triplet state as the reference. The triplet reaction pathway (purple line) begins with the formation of a hydrogen bond between the $^3O_2$ and the AHQ molecule resulting in an energy of -0.11 eV. The first hydrogen abstraction to the leading oxygen has a transition state energy of 0.17 eV. At some point the total spin must decrease since there is an energetic penalty to form H_2O_2 in the triplet state while it is energetically favorable to form H_2O_2 in the singlet state. Upon completion of the first hydrogen abstraction is when we predict the total spin to reduce to zero. This is based on how after the first hydrogen abstraction, the singlet and triplet state share similar energies (triplet: 0.14 eV; singlet: 0.15 eV) and they share similar positions. This does not occur again during the mechanism. From here, now in the singlet state (gold line), the OOH· rotates around the hydrogen bond formed between it and the partially dehydrogenated AHQ molecule (pAHQ) to present the other O atom towards the other OH-group on the pAHQ molecule. This is a barrierless transition that raises the energy of the system to 0.20 eV. This rotated state is what is illustrated in Figure 2. Then the OOH· transitions across the molecule and forms a bond with the carbon adjacent to the other OH-group. The energy of the transition state is 0.53 eV and the resulting intermediate has an energy of -0.80 eV. The energy of the transition state to break this carbon-oxygen bond and abstract the second hydrogen is at 0.16 eV and the energy of the resulting H_2O_2 molecule hydrogen bonded to the dehydrogenated AHQ molecule is -1.07 eV.

The identified location, just after the first hydrogen abstraction, is the most likely location for the total spin to reduce from 1 to 0 as there is a convergence in geometry and energy of the two states. Figure S1 in the supplemental information shows an expanded figure where four reaction pathways are illustrated: the two shown in Figure 2, the triplet pathway with the trailing oxygen in the OOH· hydrogenated, and the singlet pathway with the front oxygen in the OOH· hydrogenated. After the identified location where the total spin can relax from 1 to 0 the four pathways diverge in terms of energy and position. Thus it is unlikely that the transition between triplet and singlet states occurs at any other part of the reaction since it would probably involve some sort of electromagnetic emission which has not been previously reported.

Two dashed lines are included in Figure 2 and represent the separated OOH· molecule from the partially dehydrogenated AHQ. These thresholds are probably overestimated given that no entropic contributions are included in this reported result. The implication is that if these entropic contributions are large, it may still be favorable for the OOH· radical to escape. In a previous description of the AHQ process[28] they state that this process follows a free-radical chain mechanism[39] that involves two separate
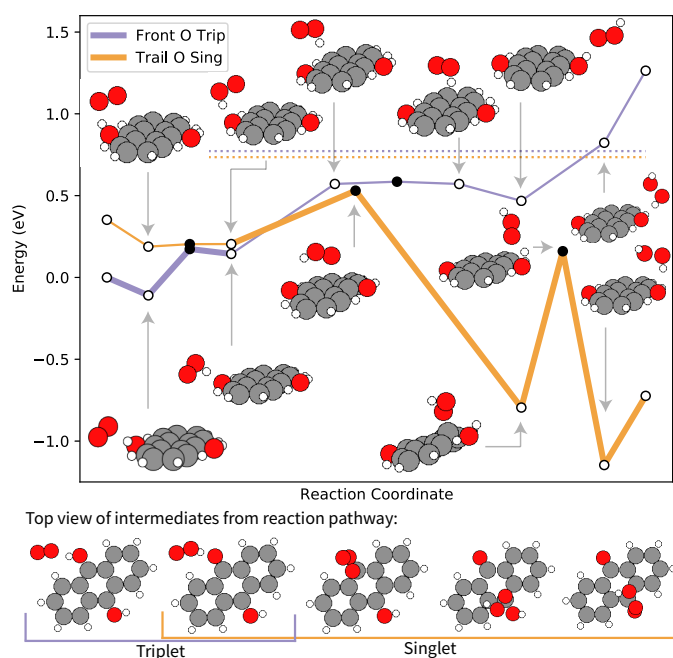
Fig. 2 The most favorable AHQ reaction pathway (outlined with bold lines) calculated for the reduction of O_2 to H_2O_2. Triplet spin calculations are in purple while singlet spin calculations are in gold. The path starts in the triplet state and the first hydrogen atom is abstracted to form $OOH^{\cdot}$. Then the $OOH \cdot$ reduces its total spin to 0 given that the triplet and singlet states are the same energy in this configuration. Then the $OOH^{\cdot}$ spins to present the unhydrogenated O atom and transitions across the AHQ to eventually become H_2O_2. Intermediates are indicated by the white dots, while transition states are indicated by black dots.

AHQ molecules to form H_2O_2. However, in this description the starting catalyst has additional hydrogenation at the 9, and 10 position on the ring. In a more recent description of the industrial process[29] it is reported that additional hydrogenation tends to occur at the 5, 6, 7, and 8 position to a much greater degree and results in a less active catalyst than if the anthracene moiety was unsaturated. If the entropic contributions are small, the reduction of O_2 to H_2O_2 should stay on the same AHQ molecule as it is not energetically favourable for the $OOH^{\cdot}$ radical to separate from the catalyst. To explore this possibility, we will assume that the entropic contributions are small and that the process involves only one AHQ molecule.

The results reported here are consistent with with the previously reported pathway by Nishimi et al.[2] when the difference in the reference state is taken into account. This includes considering a pathway where the $OOH^{\cdot}$ by-passes the deep potential energy minimum and forms a hydrogen bond with the second OH-group. In our calculations, no hydrogen bond could be formed and the hydrogen abstraction was always a barrierless process. This indicates that if the $OOH^{\cdot}$ species were to avoid the newly reported minimum that it should be facile for it to abstract the second hydrogen. In their calculations, Nishimi et al. also reported no barrier for this process. One notable exception is that in this work we were unable to calculate an intermediate where $OOH^{\cdot}$ formed a hydrogen bond with the remaining OH-group in the singlet state. Every attempt resulted in either no association

with the OH-group or the formation of H_2O_2. In our case, stable $OOH^{\cdot}$ states were calculated above the partially dehydrogenated AHQ molecule halfway between the C=O and C−OH groups had the same energy as their reported case for the $OOH^{\cdot}$ hydrogen-bonded to the second OH-group.

The major difference between this work and what was presented by Nishimi et al. is that along the most favorable pathway presented in Figure 2 is a deep potential well where the $OOH^{\cdot}$ absorbs on to the carbon atom adjacent to the second OH-group. Nishimi et al. reported no information on the transition along the AHQ molecule after the first hydrogen abstraction[2]. This calculated pathway serves as an extension to their work and demonstrates that there is a location where the reaction falls into a significant potential energy well. The appearance of this major binding site for the $OOH^{\cdot}$ radical is explained by the same work of Nishimi et al. where they identify a molecular orbital at the location of that carbon atom after the first hydrogen abstraction that could adsorb the radical as it transitions across the surface.

In general, the H_2O_2 synthesis mechanism is typically described as a radical chain sequence, and there are many side products which may be produced and consumed in the overall process. For example, the frequently cited representation of the synthesis of H_2O_2 using 9,10-dihydroxy-9,10-dihydroanthracene published by Campos-Martin et al. illustrate one proposed mechanism with many side products[28]. In a recent paper, Korth and Mulder[31] argues that the previously calculated activation barrier for the first hydrogen abstraction by Nishimi et al.[2], which is proposed to be the rate determining step is too small. Korth and Mulder estimate that the rate of the reaction based on the Nishimi et al. barrier is 1.4×10^6 M^{-1} s^{-1}. Korth and Mulder argue that the speed at which that reaction proceeds would make the rate of dissolution of O_2 into the solvent the rate-limiting process. O_2 dissolution has not been reported in the literature as the rate-limiting process which implies that the rate determining step must have a larger barrier. In its place, based on many other hydrogen abstraction processes by $^3O_2$ and $HO_2 \cdot$ from arenols, aryloxyls and their tautomers, they suggest that 10-Hydroxy-9(10H)-anthracenone, a tautomer of AHQ, plays a significant role in the synthesis of H_2O_2. 10-Hydroxy-9(10H)-anthracenone has a similar structure as the stable intermediate that is reported in this paper in regards to the carbon at the 10 position being active towards forming bonds with absorbates once the H-atom is abstracted from the OH-group at the 9 position. Korth and Mulder suggest that the absorbate is the H-atom from the OH-group at the 9 position while in this work's case it is the hydroperoxyl radical. Of note, our calculated pathway does not involve a tautomerization reaction. Instead, our proposed H_2O_2 peroxide synthesis reaction produces a similar type of structure to 10-Hydroxy-9(10H)-anthracenone as a part of the mechanism instead of relying on hydrogen atoms transferring across the AHQ molecule. The 0.27 eV difference between our suggested intermediate and the formation of H_2O_2 provides enough of a thermodynamic driving force to complete the reaction. Additionally, the 0.96 eV activation energy between the intermediate and H_2O_2 formation also eliminates the concern that the first hydrogen abstraction step is too shallow to account for the dissolution of O_2 being the rate determining step. Finally,

similar adducts have also been calculated by Valgimigli *et al.*[40] for hydrogen abstraction by O_2 from 1,4-semiquinone.

Given the potential for the OOH$^{\cdot}$ radical in the favorable singlet state to be trapped in a deep potential well during the reaction, a search was performed to determine alternative small carbon-based catalysts that eliminate the need for a potential transit across the catalyst. Twelve alternatives were tested where the two OH-groups, or one OH-group and an acidic C−H (as is the case for 11H-benzo[a]fluorene-10-diol) located on the same side of the each molecule. These twelve molecules were selected as all of them can exist with hydrogenated and dehydrogenated OH-groups like AHQ and AQ. The results of triplet and singlet state calculations for the hydrogenated catalyst with a separated O_2 molecule and the dehydrogenated catalyst with a separated H_2O_2 molecule are presented in Figure 3. Both spin states for both physical states are presented for reference.

Based on this search only two molecules present themselves as potential alternatives based on the energy of the singlet state calculation of the dehydrogenated catalyst with a separated H_2O_2 molecule relative to the triplet state calculation of the hydrogenated molecule with a separated O_2 molecule: phenanthrene-9,10-diol and benzo[c]phenanthrene-1,11-diol. Benzo[c]phenanthrene-1,11-diol is the only molecule which resulted in an exothermic energy difference, however, when benzo[c]phenanthrene-1,11-diol is dehydrogenated one of the oxygen atoms interacts with an adjacent carbon atom to close the ring. It is assumed that this ring closure will not be facile to reopen to regenerate the catalyst so it is disregarded. The other candidate, phenanthrene-9,10-diol, is essentially energetically equivalent for both the separated reactant case and separated product case. However, a similar motif has recently been credited for high electrochemical activity of graphene edges for H_2O_2 synthesis[41].

A full reaction pathway was calculated for the singlet and triplet pathways for the conversion of $^3O_2$ to H_2O_2 with phenanthrene-9,10-diol. This is illustrated in Figure 4. As before, the system begins in the triplet state and is indicated by the purple line in the figure. All the following energies are relative to the separated $^3O_2$ and phenanthrene-9,10-diol molecules in the triplet state. The reaction starts by $^3O_2$ forming a hydrogen bond with an OH-group over top of the phenanthrene-9,10-diol molecule with an energy of -0.12 eV. The energy of the transition state to abstract the first hydrogen atom is 0.25 eV and the energy of the resulting OOH$^{\cdot}$ radical is 0.15 eV. As the first hydrogen is abstracted the O_2 translates to in front of the phenanthrene molecule. In the singlet state reaction pathway, however, the OOH$^{\cdot}$ molecule remains above the phenanthrene molecule. The shift in position of the OOH$^{\cdot}$ moiety in the triplet state means that there is no early location for the total spin to drop from 1 to 0, like in the AHQ case, as there is no overlap of both energy of the system and the positions of the molecules until much later in the reaction. This includes the transition states for both the singlet and triplet pathway for the first hydrogen abstraction: while they both have similar energies, the molecules are in different places. Moving forward along the reaction pathway, as the OOH$^{\cdot}$ begins the second hydrogen abstraction, the energy of the triplet

and singlet states converge. The blue point on the plot at 0.62 eV illustrates where both the energy and position of both states overlap. From here the total spin of the system can drop to 0 and relax to form H_2O_2 in the singlet state which has an energy of -0.33 eV.

Placing both OH-groups on the same side of the molecule seems to have the intended result during the synthesis of H_2O_2 where the hydroperoxyl radical does not interact with the carbon atoms on the phenanthrene backbone to form a stable intermediate that can kinetically inhibit the reaction. The reaction takes place primarily in the triplet state where we have not been able to calculate a stable complex between the OOH$^{\cdot}$ and the phenanthrene backbone. Additionally, the reaction occurs in front of the two OH-groups meaning that the OOH$^{\cdot}$ moiety is also physically separated from the phenanthrene backbone.

Based on the above reaction pathway, the formation of H_2O_2 is exothermic. Relative to the separated O_2 molecule in the triplet state, the total energy of the system drops to -0.33 eV for the adsorbed H_2O_2 molecule in the singlet state. This is important since this process is driven thermodynamically towards the H_2O_2 production. Extraction of the H_2O_2 might be a little challenging given that the energy of the separated H_2O_2 from the phenanthrene-9,10-dione molecule is 0.01 eV higher than the separated $^3O_2$/phenanthrene-9,10-diol. At 298.15 K and 1 atm, the $\Delta_r G$ calculated using the ideal gas limit for the separated reactants to the separated products is 0.08 eV. This results in an equilibrium constant, K, of 0.05. However, the minimum energy state along the reaction pathway is H_2O_2 adsorbed on phenanthrene-9,10-dione. Therefore, the system would spontaneously form this state and produce H_2O_2. Once that occurs, the reaction conditions could change such that the barrier of the reverse reaction would inhibit O_2 formation so that the H_2O_2 could be extracted. However, one additional consideration is that in the singlet state a complex between the OOH$^{\cdot}$ and carbon on the phenanthrene backbone with the OH-group does for a stable complex with an energy of -0.59 eV relative to the reference state. Is is thermodynamically favorable that instead of separating from the phenanthrene-9,10-dione, the H_2O_2 molecule might decompose, returning one Hydrogen atom to an oxygen atom on the phenanthrene backbone and the remaining OOH$^{\cdot}$ moiety forming a complex with the carbon adjacent to the newly formed OH-group. It is expected that there would be a large barrier, similar to the AHQ reaction, that could kinetically prevent this from happening.

One interesting result from the above calculated pathway is that H_2O_2 could also decompose into $^1O_2$. The lowest energy gold (singlet) pathway does not have a point where the energy and position of both molecules in the system overlap with the triplet state pathway. This means that the most favourable reverse reaction would result in singlet O_2 being produced. This result has been observed with carbocatalysts in the literature. The chemiluminescence phenomenon of luminol can be performed with H_2O_2. The accepted pathway involves the decomposition of H_2O_2 into OH$^{\cdot}$ and $O_2^{\cdot-}$ radicals resulting in chemiluminescence. Wang *et al.* reported that when this process was catalyzed using graphene oxide[42], and carbon nanodots[43] the H_2O_2 was decomposed into $^1O_2$ which lead to chemiluminescence. Wu and
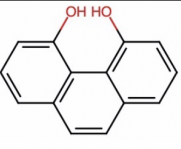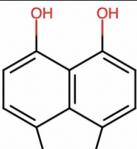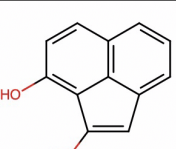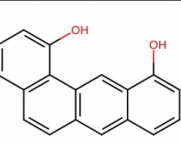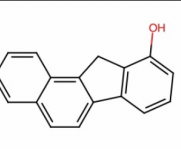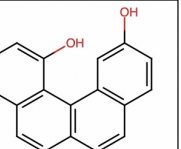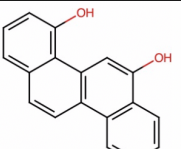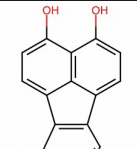
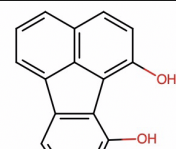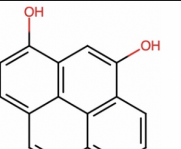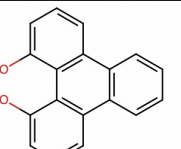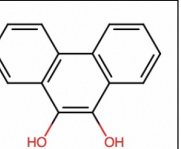|						
	phenanthrene-4,5-diol	acenaphthylene-5,6-diol	acenaphthylene-2,3-diol	benzo[a]anthracene-1,11-diol	11H-benzo[a]fluorene-10-diol	benzo[c]phenanthrene-1,11-diol
Triplet O_2 (eV)	0	0	0	0	0	0
Singlet O_2 (eV)	0.37	0.37	0.37	0.37	0.38	0.37
Triplet H_2O_2 (eV)	1.57	1.54	1.09	1.18	1.51	1.38
Singlet H_2O_2 (eV)	1.40	1.23	0.76	1.04	0.53	-0.41
	chrysene-4,6-diol	fluoranthene-3,4-diol	fluoranthene-1,10-diol	pyrene-1,9-diol	triphenylene-4,5-diol	phenanthrene-9,10-diol
Triplet O_2 (eV)	0	0	0	0	0	0
Singlet O_2 (eV)	0.37	0.37	0.38	0.36	0.38	0.36
Triplet H_2O_2 (eV)	1.52	1.51	1.89	1.44	1.57	1.41
Singlet H_2O_2 (eV)	0.87	1.69	1.31	0.32	1.24	0.01

Fig. 3 An illustration of the molecules evaluated with the triplet and singlet energies for both the O_2 and H_2O_2 intermediates. The energies for each molecule are relative to their Triplet O_2 case. Phenanthrene-9,10-diol was determined to be the most suitable candidate to explore due to the singlet hydrogen peroxide's energy being the closest to zero. All the rest of the evaluated molecules indicated an endothermic reaction, except for benzo[c]phenanthrene-1,11-diol. Benzo[c]phenanthrene-1,11-diol was not chosen as the most suitable candidate given that when the H was abstracted from the OH a ring closed. This would make it difficult to close the catalytic cycle and reduce it so that it would be able to produce more H_2O_2.
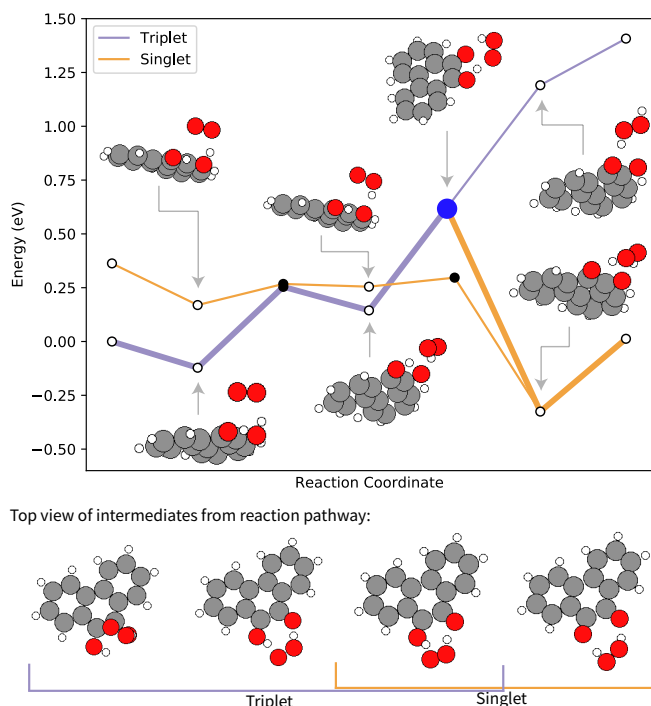
Top view of intermediates from reaction pathway:

Fig. 4 The triplet and singlet pathways for the conversion of O_2 to H_2O_2 with phenanthrene-9,10-diol. The purple line is for the triplet pathway, while the gold line is for the singlet pathway. Black and blue circles represent transition states while white circles represent relaxed intermediates.

Han also report the production of $^1O_2$ from H_2O_2 with hollow fluorescent carbon nanoparticles[44]. All of these reports state that this decomposition follows a route that involves the formation of $OH^{\cdot}$ and $O_2^{\cdot -}$ radicals instead of $OOH^{\cdot}$ radicals, however, the formation of $^1O_2$ from an oxygenated carbocatalyst provides some support for this calculated pathway.

The hydrogenation step of the AQ catalyst is the most important step in the AQ process[29]. Due to its importance the barrier for the regeneration of phenanthrene-9,10-dione was performed. The barrier is 1.29 eV and is illustrated in Figure 5. The pathway begins with the H_2 molecule in front of the two oxygen atoms on phenanthrene-9,10-dione. As the the hydrogen molecule approaches, it separates and the combined system relaxes in to the final form. A second pathway was tested where the H_2 molecule started above the molecule and resulted in an equivalent reaction pathway.

The regeneration of AQ in industrial settings uses a Pd catalyst[29]. This is because the two sites that need to be hydrogenated are distant enough that a catalyst surface is necessary to transport the two hydrogen atoms from H_2 to both sides. A DFT study by Kamachi et al. for the rehydrogenation of AQ on Pd(111) surface reported that the barriers for this two-step process are 0.6 eV and 0.7 eV for the first and second hydrogen abstractions respectively[30]. The barrier calculated for the regeneration of phenanthrene-9,10-dione is significantly larger than the values calculated for regenerating AQ over a Pd catalyst, however, using a Pd catalyst to reduce phenanthrene-9,10-dione or
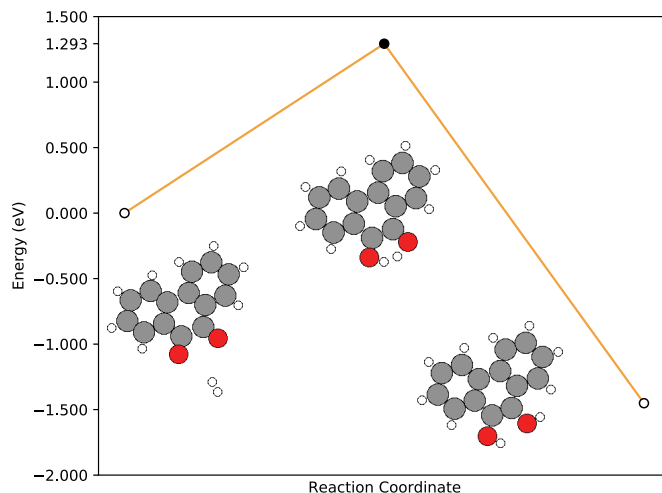

Fig. 5 Reaction pathway for the rehydrogenation of phenanthrene-9,10-dione. Black and blue circles represent transition states while white circles represent relaxed intermediates.

an alternative reducing agent to H_2 could dramatically lower this barrier. The removal of Pd from the process would be a positive step since it must be fully extracted after this catalyst regeneration step as it facilitates the breakdown of H_2O_2 in the O_2 reduction step. An alternative reducing agent might be able to take advantage of simultaneously reducing both oxygen atoms and if that process had a barrier that is comparable to that of the regeneration of AHQ with Pd would dramatically strengthen the case for phenanthrene-9,10-diol to be an alternative catalyst for H_2O_2 production. There are many possible degradation products of AQ that result from this regeneration stage, and these should be studied for phenanthrene-9,10-dione, especially in the context of different reducing agents, however, this analysis is outside of the scope of this report.

4 Conclusion

This paper presents computational results modeling the transition of $OOH^{\cdot}$ across the AHQ molecule and explore alternative catalysts to eliminate the transition. For the AHQ process, it is favorable for the hydroperoxyl to move across the AHQ molecule and fall into a deep well that will slow down the reaction. Based on the previously calculated pathway, the rate determining step was proposed to be too small meaning that O_2 dissolution would be the rate limiting factor. This new minima helps to clarify how this is not the case. Alternative molecules which place OH-groups on the same side of similarly sized molecules were explored to determine if a suitable alternative exists where the O_2 molecule can be fully reduced in the same location. Multiple molecules were surveyed, and phenanthrene-9,10-diol was selected for further analysis. The reaction barriers for phenanthrene-9,10-diol were found to be smaller in comparison to those of the AHQ molecule. Regeneration of phenanthrene-9,10-dione with H_2 had higher barriers than what was previously reported for the reduction of AQ, however, this is without a Pd catalyst that is common to AQ reduction. Being able to reduce phenanthrene-9,10-dione without the need of a Pd catalyst does present an improvement over the current

AQ process since this catalyst must be completely removed so the regenerated catalyst can be used to synthesize H_2O_2.

Conflicts of interest

There are no conflicts to declare.

Acknowledgements

Notes and references

1 N. Sharma, N. K. Bhardwaj and R. B. P. Singh, *J. Cleaner Prod.*, 2020, **256**, 1–11.

2 T. Nishimi, T. Kamachi, K. Kato, T. Kato and K. Yoshizawa, *Eur. J. Org. Chem.*, 2011, **2011**, 4113–4120.

3 R. Ciriminna, L. Albanese, F. Meneguzzo and M. Pagliaro, *ChemSusChem*, 2016, **9**, 3374–3381.

4 X. Tong, W. Shen, X. Chen and J.-P. Corriou, *J. Cleaner Prod.*, 2018, **198**, 1066–1075.

5 F. Lopez, M. Diaz, M. Eugenio, J. Ariza, A. Rodriguez and J. L., *Bioresour. Technol.*, 2003, **87**, 255–261.

6 C. Samanta, *Appl. Catal., A*, 2008, **350**, 133–149.

7 W. Wang, X. Lu, P. Su, Y. Li, J. Cai, Q. Zhang, M. Zhou and O. Arotiba, *Chemosphere*, 2020, **259**, 127423.

8 Y.-f. Zhang, S.-y. Zhang, H. Li, C.-w. Wang, F.-h. Jiang and J.-f. Lyu, *Chemosphere*, 2020, **257**, 127140.

9 J. Teles, I. Hermans, G. Franz and R. Sheldon, *Oxidation*, Wiley, 2015, pp. 11–20.

10 C. Miao, Q. Zhu, Y. Yi, J. Su, N. He, J. Liu and H. Guo, *Ind. Eng. Chem. Res.*, 2019, **58**, 11739–11749.

11 G. Blanco-Brieva, M. Pilar de Frutos-Escrig, H. Martín, J. Campos-Martin and J. Fierro, *Catal. Today*, 2012, **187**, 168–172.

12 S. Fukuzumi, Y. Yamada and K. Karlin, *Electrochim. Acta*, 2012, **82**, 493–511.

13 E. Jung, H. Shin, W. Hooch Antink, Y.-E. Sung and T. Hyeon, *ACS Energy Lett.*, 2020, **5**, 1881–1892.

14 J. S. Jirkovský, I. Panas, E. Ahlberg, M. Halasa, S. Romani and D. J. Schiffrin, *J. Am. Chem. Soc.*, 2011, **133**, 19432–19441.

15 S. Siahrostami, A. Verdaguer-Casadevall, M. Karamad, D. Deiana, P. Malacrida, B. Wickman, M. Escudero-Escribano, E. A. Paoli, R. Frydendal, T. W. Hansen, I. Chorkendorff, I. E. L. Stephens and J. Rossmeisl, *Nat. Mater.*, 2013, **12**, 1137–1143.

16 A. Verdaguer-Casadevall, D. Deiana, M. Karamad, S. Siahrostami, P. Malacrida, T. W. Hansen, J. Rossmeisl, I. Chorkendorff and I. E. L. Stephens, *Nano Lett.*, 2014, **14**, 1603–1608.

17 E. Jung, H. Shin, B.-H. Lee, V. Efremov, S. Lee, H. S. Lee, J. Kim, W. Hooch Antink, S. Park, K.-S. Lee, S.-P. Cho, J. S. Yoo, Y.-E. Sung and T. Hyeon, *Nat. Mater.*, 2020, **19**, 436–442.

18 H. Yang, M. Zhou, W. Yang, G. Ren and L. Ma, *Chemosphere*, 2018, **206**, 439 – 446.

19 H. W. Kim, M. B. Ross, N. Kornienko, L. Zhang, J. Guo, P. Yang and B. D. McCloskey, *Nat. Catal.*, 2018, **1**, 282–290.

20 Z. Lu, G. Chen, S. Siahrostami, Z. Chen, K. Liu, J. Xie, L. Liao, T. Wu, D. Lin, Y. Liu, T. F. Jaramillo, J. K. Nørskov and Y. Cui, *Nat. Catal.*, 2018, **1**, 156–162.

21 C. Xia, S. Back, S. Ringe, K. Jiang, F. Chen, X. Sun, S. Siahrostami, K. Chan and H. Wang, *Nat. Catal.*, 2020, **3**, 125–134.

22 C. Xia, Y. Xia, P. Zhu, L. Fan and H. Wang, *Science*, 2019, **366**, 226–231.

23 P. Landon, P. J. Collier, A. F. Carley, D. Chadwick, A. J. Papworth, A. Burrows, C. J. Kiely and G. J. Hutchings, *Phys. Chem. Chem. Phys.*, 2003, **5**, 1917–1923.

24 J. Zhou, H. Guo, X. Wang, M. Guo, J. Zhao, L. Chen and W. Gong, *Chem. Commun.*, 2005, 1631–1633.

25 Y. Yi, J. Zhou, H. Guo, J. Zhao, J. Su, L. Wang, X. Wang and W. Gong, *Angew. Chem., Int. Ed.*, 2013, **52**, 8446–8449.

26 Y. Yi, J. Zhou, T. Gao, H. Guo, J. Zhou and J. Zhang, *AIChE J.*, 2014, **60**, 415–419.

27 Y. Yi, L. Wang, G. Li and H. Guo, *Catal. Sci. Technol.*, 2016, **6**, 1593–1610.

28 J. M. Campos-Martin, G. Blanco-Brieva and J. L. G. Fierro, *Angew. Chem., Int. Ed.*, 2006, **45**, 6962–6984.

29 G. Goor, J. Glenneberg, S. Jacobi, J. Dadabhoy and E. Candido, in *Hydrogen Peroxide*, in Ullmann's Encyclopedia of Industrial Chemistry, 2019, pp. 1–40.

30 T. Kamachi, T. Ogata, E. Mori, K. Iura, N. Okuda, M. Nagata and K. Yoshizawa, *J. Phys. Chem. C*, 2015, **119**, 8748–8754.

31 H.-G. Korth and P. Mulder, *The Journal of Organic Chemistry*, 2020, **85**, 2560–2574.

32 J. J. Mortensen, L. B. Hansen and K. W. Jacobsen, *Phys. Rev. B*, 2005, **71**, 035109.

33 J. Enkovaara, C. Rostgaard, J. J. Mortensen, J. Chen, M. Dułak, L. Ferrighi, J. Gavnholt, C. Glinsvad, V. Haikola, H. A. Hansen, H. H. Kristoffersen, M. Kuisma, A. H. Larsen, L. Lehtovaara, M. Ljungberg, O. Lopez-Acevedo, P. G. Moses, J. Ojanen, T. Olsen, V. Petzold, N. A. Romero, J. Stausholm-Møller, M. Strange, G. A. Tritsaris, M. Vanin, M. Walter, B. Hammer, H. Häkkinen, G. K. H. Madsen, R. M. Nieminen, J. K. Nørskov, M. Puska, T. T. Rantala, J. Schiøtz, K. S. Thygesen and K. W. Jacobsen, *J. Phys.: Condens. Matter*, 2010, **22**, 253202.

34 A. H. Larsen, J. J. Mortensen, J. Blomqvist, I. E. Castelli, R. Christensen, M. Dułak, J. Friis, M. N. Groves, B. Hammer, C. Hargus, E. D. Hermes, P. C. Jennings, P. B. Jensen, J. Kermode, J. R. Kitchin, E. L. Kolsbjerg, J. Kubal, K. Kaasbjerg, S. Lysgaard, J. B. Maronsson, T. Maxson, T. Olsen, L. Pastewka, A. Peterson, C. Rostgaard, J. Schiøtz, O. Schütt, M. Strange, K. S. Thygesen, T. Vegge, L. Vilhelmsen, M. Wal-

ter, Z. Zeng and K. W. Jacobsen, *J. Phys.: Condens. Matter*, 2017, **29**, 273002.

35 J. P. Perdew, K. Burke and M. Ernzerhof, *Phys. Rev. Lett.*, 1996, **77**, 3865–3868.

36 A. Tkatchenko and M. Scheffler, *Phys. Rev. Lett.*, 2009, **102**, 073005.

37 G. Henkelman, B. P. Uberuaga and H. Jónsson, *J. Chem. Phys.*, 2000, **113**, 9901–9904.

38 E. L. Kolsbjerg, M. N. Groves and B. Hammer, *J. Chem. Phys.*, 2016, **145**, 094107.

39 R. A. Sheldon and J. K. Kochi, *Metal-catalyzed Oxidations of Organic Compounds*, Academic Press, 1981, pp. 17 – 32.

40 L. Valgimigli, R. Amorati, M. G. Fumo, G. A. DiLabio, G. F. Pedulli, K. U. Ingold and D. A. Pratt, *The Journal of Organic Chemistry*, 2008, **73**, 1830–1841.

41 G.-F. Han, F. Li, W. Zou, M. Karamad, J.-P. Jeon, S.-W. Kim, S.-J. Kim, Y. Bu, Z. Fu, Y. Lu, S. Siahrostami and J.-B. Baek, *Nat. Commun.*, 2020, **11**, 2209.

42 D. M. Wang, Y. Zhang, L. L. Zheng, X. X. Yang, Y. Wang and C. Z. Huang, *J. Phys. Chem. C*, 2012, **116**, 21622–21628.

43 D. M. Wang, M. X. Gao, P. F. Gao, H. Yang and C. Z. Huang, *J. Phys. Chem. C*, 2013, **117**, 19219–19225.

44 Y. Wu and S. Han, *J. Lumin.*, 2016, **179**, 595 – 601.

45 J. Towns, T. Cockerill, M. Dahan, I. Foster, K. Gaither, A. Grimshaw, V. Hazlewood, S. Lathrop, D. Lifka, G. D. Peterson, R. Roskies, J. Scott and N. Wilkins-Diehr, *Comput. Sci. Eng.*, 2014, **16**, 62–74.